Contents lists available at ScienceDirect

Chemical Engineering Research and Design

journal homepage: www.elsevier.com/locate/cherd

Facile preparation of highly efficient CuO-ZnO-ZrO_2/HZSM-5 bifunctional catalyst for one-step CO_2 hydrogenation to dimethyl ether: Influence of calcination temperature

Luyang Li, Dongsen Mao, Jie Xiao, Li Li, Xiaoming Guo, Jun Yu*

Research Institute of Applied Catalysis, School of Chemical and Environmental Engineering, Shanghai Institute of Technology, Shanghai 201418, PR China

ARTICLE INFO

Article history:
Received 12 November 2015
Received in revised form 5 April 2016
Accepted 20 April 2016
Available online 6 May 2016

Keywords:
Solid-state reaction
CuO-ZnO-ZrO_2/HZSM-5
Bifunctional catalyst
CO_2 hydrogenation
Dimethyl ether

ABSTRACT

CuO-ZnO-ZrO_2/HZSM-5 bifunctional catalysts were prepared by a facile route of solid-state reaction and tested for one-step synthesis of dimethyl ether (DME) from CO_2 hydrogenation. The effects of calcination temperature (300–600 °C) on the physicochemical and catalytic properties of the bifunctional catalysts were investigated by XRD, N_2 adsorption, XPS, N_2O chemisorption, SEM, H_2-TPR, NH_3-TPD, and CO_2-TPD techniques. The results show that both the CO_2 conversion and DME selectivity of the bifunctional catalysts decrease with the increase in calcination temperature, which can mainly be attributed to the decrease of metallic copper surface area (S_{Cu}), adsorption capacity of CO_2, specific surface area, and reducibility of CuO.

1. Introduction

In recent years, the greenhouse effect caused by CO_2 is increasingly significant, and CO_2 recycling is the focus of governments and the scientific research personnel (Centi et al., 2013; Kondratenko et al., 2013; Olah, 2013). Dimethyl ether (DME) is considered to be an ideal clean fuel and a valuable starting material for the production of a range of chemicals (Mao et al., 2005; Semelsberger et al., 2006; Allahyari et al., 2014). Direct synthesis of DME from catalytic hydrogenation of CO_2 is of great economical and environmental importance, not only to synthesize useful fuels and chemical products, which will make full use of CO_2 more efficiently, but also to reduce the greenhouse effect resulted from CO_2 (Najafabadi, 2013; Pontzen et al., 2011; Wang et al., 2011).

Direct synthesis of DME from CO_2 hydrogenation is accomplished through two consecutive reactions (methanol synthesis and methanol dehydration) in one reactor via a bifunctional catalyst (Park et al., 1995; Wang et al., 2009; Zha et al., 2012, 2013; Liu et al., 2013, 2015; Zhang et al., 2014a; Witoon et al., 2015), which is generally composed of a methanol synthesis catalyst (typically Cu-based oxides) and a methanol dehydration catalyst (typically Al_2O_3 or zeolites). Among them, CuO-ZnO-ZrO_2/HZSM-5 system has been considered to be a promising catalyst for CO_2-to-DME process (Ge et al., 1999; Arena et al., 2004; Bonura et al., 2013, 2014; Frusteri et al., 2015a,b).

Presently, the CuO-ZnO-ZrO_2/HZSM-5 bifunctional catalysts are generally prepared by physical or mechanical mixing method (Arena et al., 2004; Bonura et al., 2013, 2014), which

* *Corresponding author*. Tel.: +86 21 6087 3625; fax: +86 21 6087 3625.
E-mail address: dsmao@sit.edu.cn (D. Mao).
http://dx.doi.org/10.1016/j.cherd.2016.04.018

cannot integrate CuO-ZnO-ZrO_2 and HZSM-5 effectively. But high dispersion among the components is more conducive to mutual reactions for the multi-functional integration, so to realize a more efficient mass transfer rate from the metal–oxide sites for methanol synthesis to the acid sites for methanol dehydration (Frusteri et al., 2015a). For this, some other methods such as precipitation-deposition are also used to prepare the CuO-ZnO-ZrO_2/HZSM-5 bifunctional catalysts (Frusteri et al., 2015a,b). However, HZSM-5 combines with metal ions to generate CuZSM-5 or NaZSM-5 which reduces the number of surface acid sites, subsequently leading to the disconnection between the methanol synthesis and methanol dehydration catalysts (Zhang et al., 2013). As a result, its activity is significantly lower than that of the catalyst prepared by physical mixing method (Zhang et al., 2013). Therefore, the development of a novel and effective method for the preparation of high-performance CuO-ZnO-ZrO_2/HZSM-5 catalyst is of great importance.

Solid-state synthesis has attracted extensive research interest because it is a simple, rapid, solvent-free, and energy-saving process (Ye et al., 1999). Up to now, this method has been widely used in the preparation of metal oxides and mixed metal oxides (Wang et al., 2007; Guo et al., 2009; Shi et al., 2013; Fu et al., 2015), but it has not yet been reported for the preparation of bifunctional catalyst, to our best knowledge. In this paper, CuO-ZnO-ZrO_2/HZSM-5 bifunctional catalysts were prepared by one-step solid-state synthesis for the first time. Since the calcination process is a very important step in the route of solid-state synthesis (Guo et al., 2009), the effect of calcination temperature on the catalytic performance of the derived CuO-ZnO-ZrO_2/HZSM-5 bifunctional catalysts for DME synthesis directly from CO_2 hydrogenation was investigated. The physicochemical properties of the as-prepared catalysts before or after in situ reduction were extensively characterized by XRD, N_2 adsorption, XPS, N_2O chemisorption, TPR, NH_3-TPD, CO_2-TPD, and SEM techniques, and related to the catalytic performance.

2. Experimental

2.1. Catalyst preparation

All the reactants are of analytical grade and were used without further purification or modification. Firstly, calculated amounts of $Cu(NO_3)_2{\cdot}3H_2O$, $Zn(NO_3)_2{\cdot}6H_2O$ and $Zr(NO_3)_4{\cdot}5H_2O$ were blended in solid state to form a homogenized premix, in which the molar ratio of Cu^{2+}, Zn^{2+} and Zr^{4+} was 0.5:0.2:0.3 based on our previous studies (Guo et al., 2010; Li et al., 2015). Then oxalic acid ($C_2H_2O_4{\cdot}2H_2O$), a ligand for metal cations, was added to the premix and ground in an agate mortar at room temperature. The molar ratio of $C_2H_2O_4{\cdot}2H_2O$ to the metal ions was 1.5:1. After being ground for ca. 30 min, all the reactants transferred to a uniform, viscous and muddy precursor for the CuO-ZnO-ZrO_2 (CZZ) catalysts. Then a commercial HZSM-5 zeolite (SiO_2/Al_2O_3 = 38, molar ratio, Nankai University Chemical Plant, China) was added to the precursor for the CZZ catalyst and mixed homogeneously. The weight ratio of CuO-ZnO-ZrO_2 to HZSM-5 was 10:1 based on our preliminary experiments. Then the precursor for the CuO-ZnO-ZrO_2/HZSM-5 bifunctional catalyst was dried at 110 °C for 12 h and calcined in air at a certain temperature (300–600 °C) for 6 h. The resulted catalysts were termed as CZZH-300, CZZH-400, CZZH-500, and CZZH-600, respectively.

In addition, for the purpose of comparison, two CuO-ZnO-ZrO_2/HZSM-5 catalysts with the same composition as described above were prepared by the most widely used mechanical mixing method (Arena et al., 2004; Bonura et al., 2013, 2014), in which CuO-ZnO-ZrO_2 catalysts were prepared by oxalate and ammonium carbonate co-precipitation as described elsewhere (Wang et al., 2007). For the sake of simplicity, these two bifunctional catalysts were named as CZZ(O) + HZ and CZZ(A) + HZ hereafter, respectively.

2.2. Catalyst testing

The catalytic performance was tested in a continuous-flow, fixed-bed reactor (Wang et al., 2009). About 0.5 g of catalyst (40–60 mesh) mixed with quartz sand was packed into the reactor. Prior to the catalytic measurements, the fresh catalyst was reduced in a stream of 10 vol.% H_2/N_2 flowing at 30 mL min^{-1} at 300 °C for 3 h under atmospheric pressure. Then the reactor was cooled to the reaction temperature and a gas mixture (CO_2:H_2:N_2 = 22:66:12, molar) was introduced, raising the pressure to 3.0 MPa. Effluent products were analyzed on-line with a gas chromatograph (GC) (6820, Agilent). Methanol and DME was determined with a Porapak Q column and a flame ionization detector (FID), and other gaseous products were determined by a Carbosieve column and a thermal conductivity detector (TCD). To avoid any condensation of the heaviest products, all transfer lines between the reactor and GC were kept at a temperature of 250 °C. Activity and products selectivity were calculated by normalization method and the steady-state values were quoted as the average of four different analyses taken after 5 h on stream operation. CO_2 conversion and the selectivity of CO, DME, CH_3OH, and the yield of DME were calculated as shown in formula (1)–(5):

$$X_{CO_2} = \frac{n_{CH_3OH} + n_{CO} + 2n_{DME}}{n_{CO_2} + n_{CH_3OH} + n_{CO} + 2n_{DME}} \quad (1)$$

$$S_{CH_3OH} = \frac{n_{CH_3OH}}{n_{CH_3OH} + n_{CO} + 2n_{DME}} \quad (2)$$

$$S_{CO} = \frac{n_{CO}}{n_{CH_3OH} + n_{CO} + 2n_{DME}} \quad (3)$$

$$S_{DME} = \frac{2n_{DME}}{n_{CH_3OH} + n_{CO} + 2n_{DME}} \quad (4)$$

$$Y_{DME} = \frac{2n_{DME}}{n_{CO_2} + n_{CH_3OH} + n_{CO} + 2n_{DME}} \quad (5)$$

where X_{CO_2} and S_X stand for the conversion of CO_2 (%) and the selectivity of product X (%), respectively; n_x represents the moles of the species X.

The space time yield (STY) of DME and CH_3OH ($mg_{DME\ or\ CH_3OH}\ g_{cat}^{-1}\ h^{-1}$) was defined as follows:

$$STY_{DME} = \frac{n_{DME}}{n_{CO_2,in} \times 0.5 \times MV \times V_{CO_2} \times MW_{DME}} \quad (6)$$

$$STY_{CH_3OH} = \frac{n_{CH_3OH}}{n_{CO_2,in} \times 0.5 \times MV \times V_{CO_2} \times MW_{CH_3OH}} \quad (7)$$

where V_{CO_2} is the volumetric flow of CO_2 ($cm^3\ min^{-1}$), MW_{CH_3OH} and MW_{DME} are the molecular weight of CH_3OH and DME ($g\ mol^{-1}$), MV is the molar volume of ideal gas, 22,400 $cm^3\ mol^{-1}$, and 0.5 is the total amount of catalysts.

2.3. Catalyst characterization

X-ray diffraction (XRD) patterns were recorded with a PANalytical X'Pert diffractometer. Two theta angles ranged from 10° to 80° with a speed of 6° min^{-1} operating with Ni β-filtered Cu Kα radiation at 40 kV and 40 mA.

BET surface area and pore volume were measured on a Micromeritics ASAP 2020 M+C adsorption apparatus at liquid N_2 temperature using N_2 as adsorbate. The specific surface area was calculated following the BET method and the pore volume was determined at a relative pressure (P/P_0) of 0.99. Before measurements, the samples were dried in situ at 200 °C for 4 h under vacuum.

The surface morphology was observed by the scanning electronic microscopy (SEM, FEI, Quanta 200 FEG). The surface compositions of the samples were investigated by X-ray photoelectron spectroscopy (XPS, Perkin-Elmer PHI 5000C ESCA) using Al Kα radiation. The C 1s = 284.6 eV was a reference for the calibration of all the binding energy values.

To characterize the reduced catalysts by N_2 adsorption, XRD and XPS, the fresh catalysts were reduced at 300 °C for 1 h in a flowing of 10 vol.% H_2/N_2 mixture. The reduced catalysts were cooled to the room temperature in the reducing gas stream, and then were put into hermetic bags and characterized as quickly as possible to reduce the exposure of them with air.

The metallic copper surface area (S_{Cu}) in the reduced catalyst was determined using a N_2O chemisorption method (Guo et al., 2010). Once the catalyst was reduced in a 10 vol.% H_2/N_2 mixture at 300 °C for 1 h, it was cooled to the chemisorption temperature (60 °C) exposing in a flowing of He. Then, a flow of 2.05 vol.% N_2O/He gas mixture was fed into the reactor. The N_2 produced by the decomposition of N_2O on the exposed Cu atoms was detected using a mass spectrometer (Pfeiffer Vacuum Quadstar, 32-bit).

Temperature-programmed reduction by H_2 (H_2-TPR) was measured in a continuous-flow apparatus. Firstly, a 30-mg catalyst sample was flushed in N_2 for 1 h. Then it was fed with a 10 vol.% H_2/N_2 mixture flowing at 30 mL min^{-1} and heated at a rate of 5 °C min^{-1}. The H_2 consumption was monitored by a TCD.

Temperature programmed desorption of NH_3 (NH_3-TPD) was carried out in a quartz tubular reactor. Firstly, the catalyst sample was reduced at 300 °C for 1 h in a flowing of 10 vol.% H_2/N_2 mixture. Then the sample was cooled to room temperature and further saturated in 10 vol.% NH_3/N_2 mixture for 1 h, followed by flushing in N_2 for 1 h. The TPD measurements were conducted in a N_2 stream (30 mL min^{-1}) from room temperature to 700 °C at a heating rate of 10 °C min^{-1}. The change of NH_3 signal was monitored by a TCD.

Temperature programmed desorption of CO_2 (CO_2-TPD) was similar to the NH_3-TPD. Prior to the adsorption of CO_2, the catalyst sample was reduced at 300 °C for 1 h by 10 vol.% H_2/N_2 mixture flowing continually. After cooling down to 50 °C, the catalyst was saturated with a 10% CO_2/N_2 mixture (30 mL min^{-1}) at this temperature for 1 h. Afterward, the TPD experiment was started with a heating rate of 10 °C min^{-1} under N_2 flow (30 mL min^{-1}), and the desorbed CO_2 was detected by a TCD.

3. Results and discussion

3.1. Catalytic performance

The catalytic performance of different Cu-ZnO-ZrO_2/HZSM-5 catalysts for one-step DME synthesis from CO_2 hydrogenation at steady state is summarized in Table 1. The major product is DME, and the side products are methanol and CO (Wang et al., 2009). As shown in Table 1, the highest CO_2 conversion and DME selectivity are found over the CZZH-300 catalyst, with values of 22.2% and 67.6%, respectively. With the increase of calcination temperature, CO_2 conversion, DME selectivity, DME yield, and STY of DME and CH_3OH all decrease monotonously; while the selectivity of methanol basically remain unchanged (8.6–9.0%). Thus, the decrease in DME selectivity is due to the increase in CO selectivity. These results clearly indicate that the performance of CuO-ZnO-ZrO_2/HZSM-5 catalysts for DME synthesis from CO_2 hydrogenation greatly depends on the catalyst calcination temperature and decreases gradually with the increase of calcination temperature in the range of 300–600 °C.

The effects of the conversion of CO_2 on the selectivity of products over the representative catalysts CZZH-300 and CZZH-600 are shown in Fig. 1. As a general observation, the selectivity to oxygenates (CH_3OH + DME) decreases while that to CO increases as CO_2 conversion increases. As well known, the synthesis of methanol (here means the sum of methanol and DME) and the reverse water-gas shift (RWGS) are the two parallel reactions involved in the CO_2 hydrogenation process. Obviously, raising reaction temperature is favorable for the reaction of RWGS because of its endothermic character. Meanwhile, compared to methanol synthesis, the RWGS reaction has a higher apparent activation energy (Melián-Cabrera et al., 2002), which means that the increase in CO production is faster than that of methanol with increase in reaction temperature. Consequently, in the temperature range of 200–250 °C, the selectivity of oxygenates decreases while that of CO increases along with the elevation of reaction temperature. Moreover, it should be noted that a significant difference can be observed between the two catalysts. Clearly, the catalyst CZZH-300 possesses evidently higher oxygenates selectivity than the catalyst CZZH-600 at the same CO_2 conversion.

Moreover, the most efficient catalyst CZZH-300 was selected for a stability measurement over a 100 h period. As

Table 1 – Performance of different Cu-ZnO-ZrO_2/HZSM-5 catalysts for direct DME synthesis from CO_2 hydrogenation.

Catalyst	CO_2 conv. (%)	Product selectivity (%)			DME yield (%)	STY (mg/(g_{cat} h))	
		DME	CH_3OH	CO		DME	CH_3OH
CZZH-300	22.2	67.6	8.6	23.8	15.0	507	89.8
CZZH-400	21.3	63.4	8.9	27.7	13.5	456	89.2
CZZH-500	20.9	63.3	9.0	27.7	13.2	446	88.5
CZZH-600	19.6	59.1	8.7	32.2	11.6	392	80.2

Reaction conditions: T = 250 °C, CO_2:H_2 = 1:3 (v/v), P = 3.0 MPa, GHSV = 3600 mL g^{-1} h^{-1}.
Experimental errors of the CO_2 conversion and product selectivity are within ±3%.

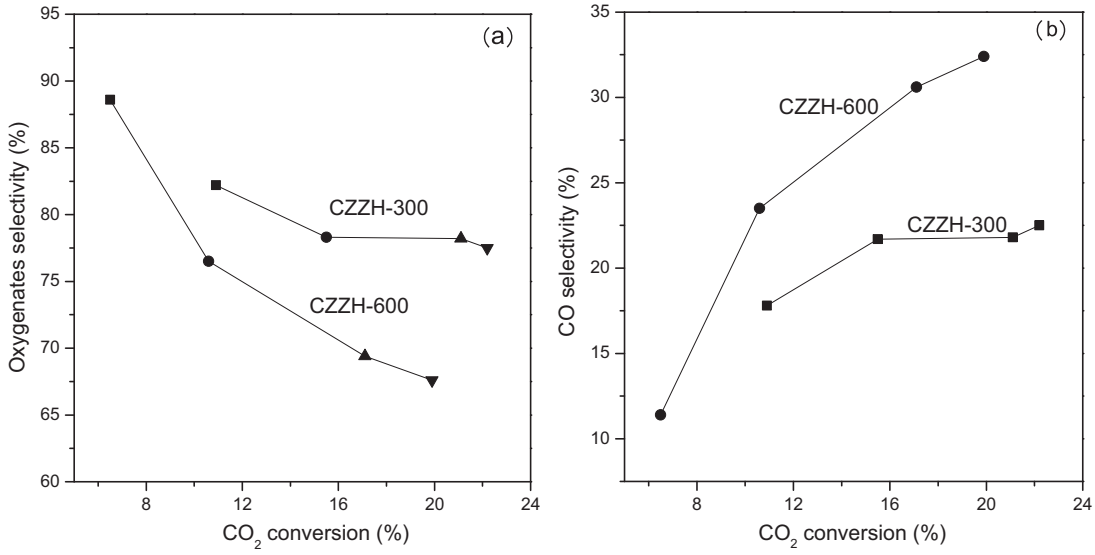

Fig. 1 – Oxygenates (CH_3OH + DME) selectivity (a) and CO selectivity (b) vs CO_2 conversion over the CZZH-300 and CZZH-600 catalysts at CO_2:H_2 = 1:3 (v/v), P = 3.0 MPa, GHSV = 3600 mL g^{-1} h^{-1}, and T = 200–250 °C.

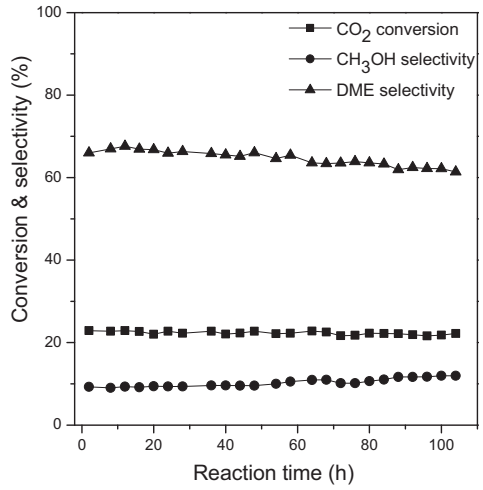

Fig. 2 – Stability of the direct synthesis of DME from CO_2/H_2 over the CZZH-300 catalyst, under the same reaction conditions as in Table 1.

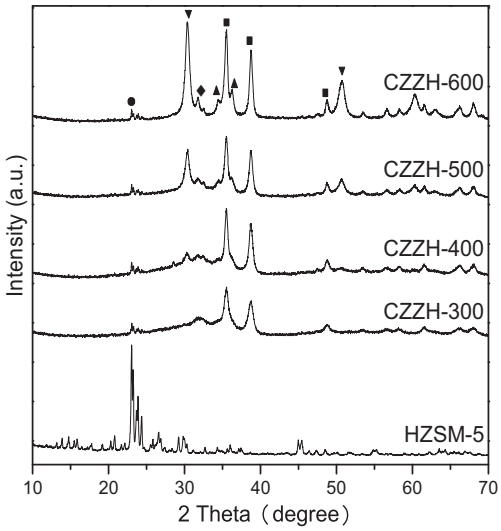

Fig. 3 – XRD patterns of HZSM-5 and different CuO-ZnO-ZrO_2/HZSM-5 catalysts: (●) HZSM-5; (■) CuO; (▲) ZnO; (▼) ZrO_2 (tetragonal); (♦) ZrO_2 (monoclinic).

shown in Fig. 2, the CO_2 conversion and the DME selectivity decreased slightly from 22.9% and 68.0% (2 h on stream) to 21.8% and 62.2%, respectively, while the methanol selectivity increased slightly from 9.2% to 11.9%. These results suggest that the main reason for the deactivation of the bifunctional catalyst is the deactivation of HZSM-5 (Tao et al., 2001). In summary, the bifunctional CZZH catalyst prepared by the present solid-sate reaction method exhibits both high catalytic activity and stability for CO_2 hydrogenation to DME.

3.2. *Textural and structural properties of the bifunctional catalysts*

Fig. 3 shows the XRD patterns of the CZZH catalysts calcined at different temperatures. As shown, the diffraction peaks ascribed to HZSM-5 between 23° and 25° (JCPDS 44-0003) appear similar in all the samples, indicating that the structure of zeolite HZSM-5 is well preserved during the preparation process and no noticeable change in crystallinity is observed when calcined at different temperatures. On the other hand, when calcined at 300 °C, only the diffraction peaks of CuO (JCPDS 80-1268) are observed at 2θ of 35.6°, 38.8° and 48.7°; while the diffraction peaks of ZnO and ZrO_2 cannot be observed distinctly, suggesting that they may have been highly dispersed or exist in a less ordered structure (Li et al., 2015). When calcination temperature is raised to 400 °C, however, there are weak diffraction lines of ZnO phase (JCPDS 36-1451) appearing at 2θ of 34.4° and 36.3°, together with the diffraction lines of both tetragonal zirconia (t-ZrO_2, 2θ = 30.3°, 50.6°, JCPDS 88-1007) and monoclinic zirconia (*m*-ZrO_2, 2θ = 31.7°, JCPDS 83-0940) (Guo et al., 2009; Li et al., 2015). Increasing the calcination temperature further to ≥500 °C, all the diffraction peaks for CuO, ZnO, and ZrO_2 become sharper and stronger, indicating an increase in the particle sizes of CuO, ZnO, and ZrO_2 crystallites and in the degree of crystallinity (Guo et al., 2009; Li et al., 2015). The mean size of CuO crystallites, which is estimated using the Scherrer equation, increases from 13.8 nm of CZZH-300 to 19.3 nm of CZZH-600 as shown in Table 2.

Fig. 4 shows the XRD patterns of different Cu-ZnO-ZrO_2/HZSM-5 catalysts after reduction at 300 °C. As seen, all the catalysts exhibit three diffraction peaks at 2θ of 43.4°, 50.8°,

Table 2 – Physicochemical properties of the different CuO-ZnO-ZrO_2/HZSM-5 bifunctional catalysts.

Catalyst	d_{CuO} [a] (nm)	S_{BET} (m^2/g)	Pore volume (cm^3/g)	Surface Cu content[b] (at.%)
CZZH-300	13.8	80.5	0.277	41.2
CZZH-400	17.2	61.0	0.186	37.9
CZZH-500	17.3	52.2	0.175	33.8
CZZH-600	19.3	41.5	0.154	29.7

[a] Determined by Scherrer's equation.
[b] Determined by XPS method.

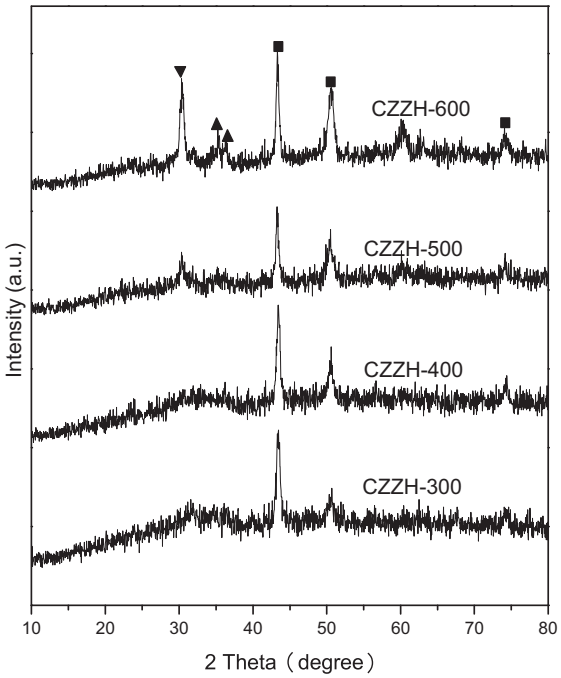

Fig. 4 – XRD patterns of different Cu-ZnO-ZrO_2/HZSM-5 catalysts after reduction at 300 °C: (■) Cu; (▲) ZnO; (▼) ZrO_2 (tetragonal).

and 73.9°, which are characteristic of the Cu(111), Cu(200) and Cu(220) planes, respectively (Li et al., 2015). Simultaneously, the diffraction lines of CuO cannot be observed any more, indicating that the CuO in the calcined samples are reduced to metallic copper. As shown in Table 3, the change trend for d_{Cu} over the reduced catalysts is the same as that for d_{CuO} over the calcined catalysts. Furthermore, the transformation of ZnO and ZrO_2 phase with the increase in calcination temperature is similar with that observed in Fig. 3.

As shown in Tables 2 and 3, the surface areas and pore volumes of both the calcined and reduced bifunctional catalysts decrease with the increase of calcination temperature, which is due to the catalysts sintering and particle size enlarging at higher temperatures, as revealed by XRD results described above. By combining Tables 1 and 3, it can be seen that both the conversion of CO_2 and selectivity to DME increase with the increment of specific surface area. Similar result was also reported by Li et al. (2014).

The S_{Cu} of the pre-reduced Cu-ZnO-ZrO_2/HZSM-5 catalysts are listed in Table 3 as well. It can be seen that the S_{Cu} decreases monotonically with the increase in calcination temperature. Since the value of S_{Cu} is a mirror of the dispersion of Cu, it can be concluded that the dispersion of Cu on the bifunctional catalysts decreases with the calcination temperature increasing (Guo et al., 2009; Li et al., 2015), which is in good agreement with the result obtained by XRD technique (Table 3).

The relative surface Cu contents of the calcined and reduced bifunctional catalysts determined by XPS measurements are presented in Tables 2 and 3, respectively. It can be seen that the relative surface Cu contents of all the catalysts are lower than the nominal one (50 at.%), which can be ascribed to enrichment of Zn and Zr on the surface of catalysts and similar results have also been reported previously (Guo et al., 2009; Li et al., 2015; Xiao et al., 2015; Słoczyński et al., 2004). On the other hand, the surface Cu contents of both calcined and reduced catalysts decrease gradually with the increase in calcination temperature, indicating that the effect of the enrichment of Zn and Zr over the surface of catalysts enhances continuously with the increase in calcination temperature (Guo et al., 2009; Li et al., 2015). This result is consistent with the S_{Cu} values described above.

Fig. 5 shows the SEM images of the bifunctional catalysts calcined at different temperatures. It can be seen that all the catalysts are in the form of irregular particles. With the increase of calcination temperature, the aggregation of the particles becomes severe, and the particle sizes of crystallites enlarge, which can be due to the particle sintering after calcination at higher temperatures. These results are in good agreement with the crystallize size calculated from the XRD analysis (see Table 2).

As well known, the activity of Cu-based catalysts for methanol synthesis from CO_2 hydrogenation depends greatly on the S_{Cu} (Guo et al., 2009, 2010; Li et al., 2015; Xiao et al., 2015; Słoczyński et al., 2004; Jun et al., 1998), although no agreement has been reached concerning the relationship between them. In this work, the relationship between the S_{Cu} and yield

Table 3 – Physicochemical properties of the reduced Cu-ZnO-ZrO_2/HZSM-5 bifunctional catalysts.

Catalyst	d_{Cu} [a] (nm)	S_{BET} (m^2/g)	Pore volume (cm^3/g)	S_{Cu} [b] (m^2/g)	Surface Cu content[c] (at.%)
CZZH-300	12.8	81.9	0.215	6.36	37.2
CZZH-400	15.5	62.9	0.199	5.75	33.2
CZZH-500	16.2	58.2	0.202	5.13	31.1
CZZH-600	18.5	51.0	0.176	4.75	23.3

[a] Determined by Scherrer's equation.
[b] Determined by N_2O chemisorption method.
[c] Determined by XPS method.

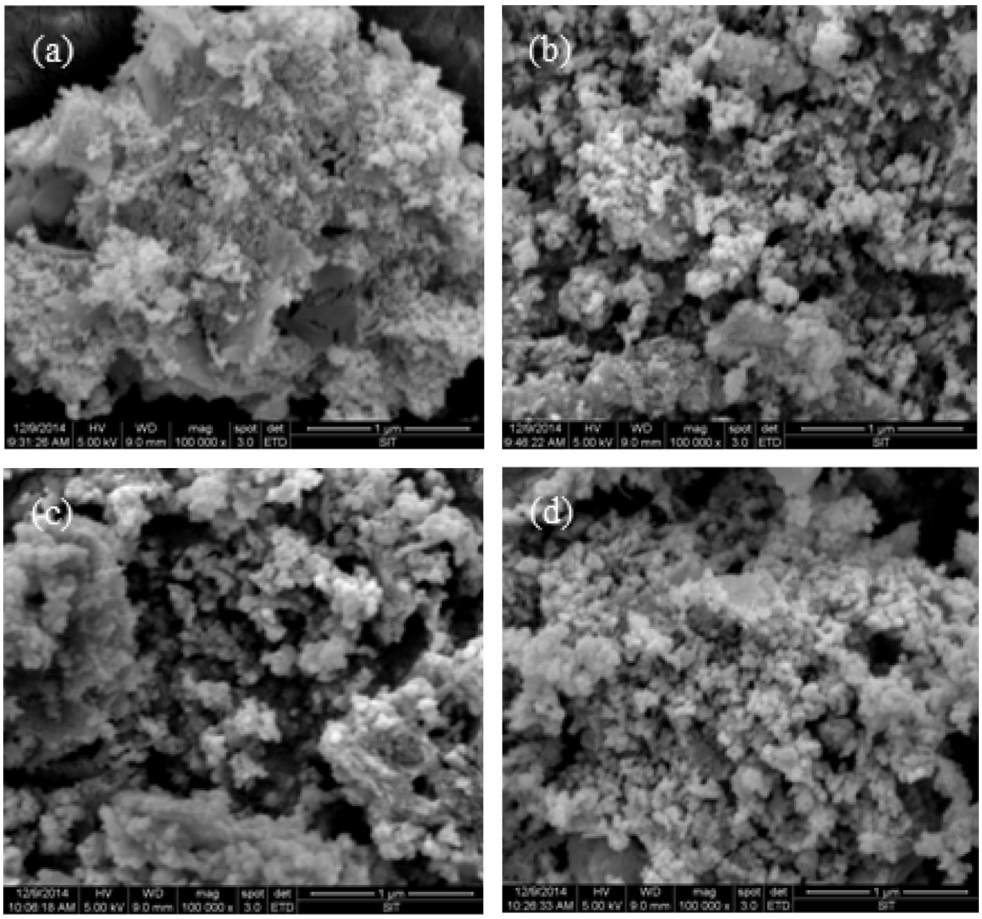

Fig. 5 – SEM pictures of the different CuO-ZnO-ZrO_2/HZSM-5 bifunctional catalysts: (a) CZZH-300, (b) CZZH-400, (c) CZZH-500, and (d) CZZH-600.

for the formation of methanol and DME ($Yield_{CH_3OH+DME}$) over the different Cu-ZnO-ZrO_2/HZSM-5 bifunctional catalysts was studied; the result is presented in Fig. 6. It can be seen that the $Yield_{CH_3OH+DME}$ increases linearly with the increase of the S_{Cu}, indicating that the decrease of $Yield_{CH_3OH+DME}$ over the catalysts calcined at higher temperatures was ascribed to the decrease of S_{Cu}. To check the possible change of active site of catalyst by the calcination temperature, turnover frequency of produced methanol and DME (methanol and DME yield per active site and per unit time, $TOF_{CH_3OH+DME}$) was obtained. The correlation between $TOF_{CH_3OH+DME}$ and the catalyst calcination temperatures is shown in Fig. 7. It is noted that the value of $TOF_{CH_3OH+DME}$ of different catalysts is nearly a constant under the present reaction conditions. This result suggests that a noticeable change of catalyst active site does not take place by the change of calcination temperature. That is, the production of methanol from CO_2 hydrogenation does not depend on

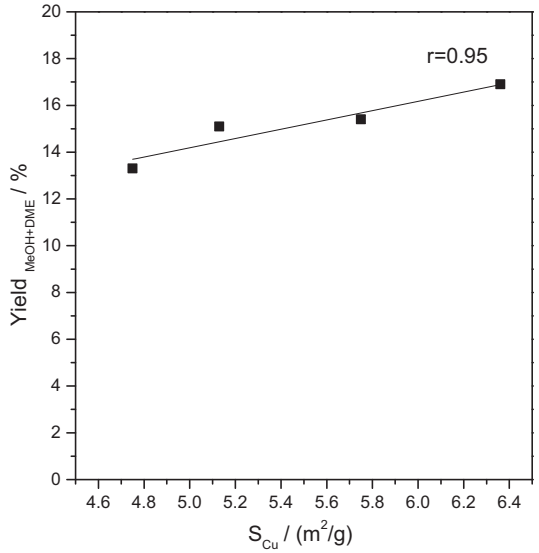

Fig. 6 – The relationship between the yield for methanol and DME and the surface area of metallic copper (S_{Cu}).

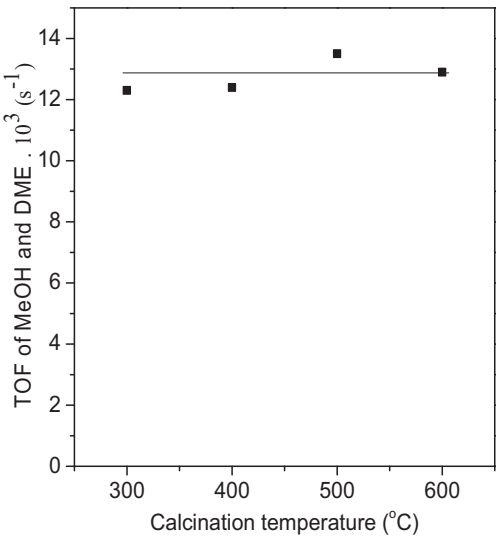

Fig. 7 – Effect of the catalyst calcination temperature on turnover frequency for methanol and DME production.

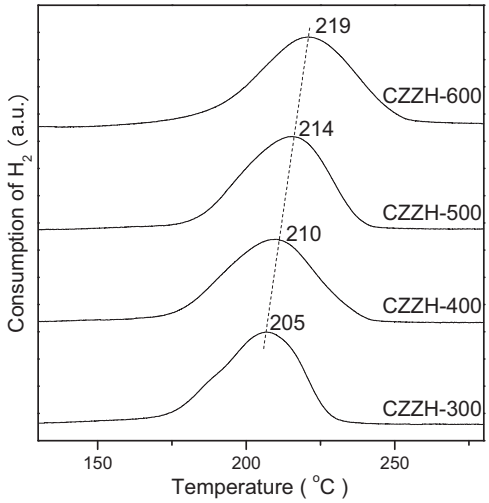

Fig. 8 – H_2-TPR profiles of different CuO-ZnO-ZrO_2/HZSM-5 bifunctional catalysts.

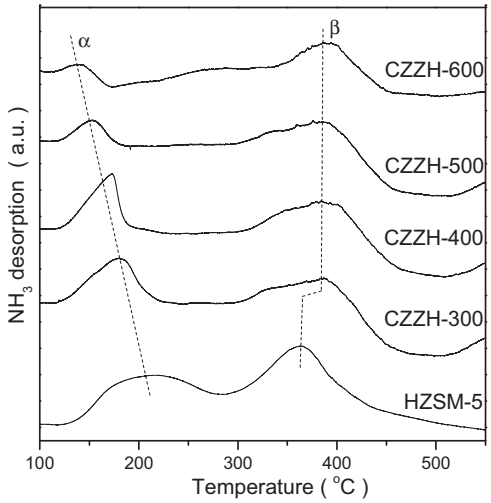

Fig. 9 – NH_3-TPD profiles of pure HZSM-5 and pre-reduced Cu-ZnO-ZrO_2/HZSM-5 bifunctional catalysts.

the Cu particle size of catalyst but mainly on the S_{Cu} (Arakawa et al., 1992).

3.3. *Reducibility of the catalysts*

The reduction behavior of the bifunctional catalysts was invested by TPR measurements and the results are shown in Fig. 8. Since ZnO and ZrO_2 cannot be reduced within the experimental region used here (Ribeiro et al., 2008), the reduction peak is related to the reduction of CuO species. As shown in Fig. 8, all the bifunctional catalysts show a similar broad peak, but the temperature of peak maximum increases in the order of CZZH-300 < CZZH-400 < CZZH-500 < CZZH-600, suggesting that the reducibility of the bifunctional catalysts decrease in the following order: CZZH-300 > CZZH-400 > CZZH-500 > CZZH-600. It was reported previously that the active and selective Cu-based catalysts for CO_2 hydrogenation to methanol show higher reducibility (Wang et al., 2009; Lee and Lee, 1995). Therefore, the orders of CO_2 conversion and total selectivity for methanol and DME over the different bifunctional catalysts are the same as the order of reducibility of the catalysts.

3.4. *Acidity of the catalysts*

The acidity of the different Cu-ZnO-ZrO_2/HZSM-5 catalysts after in situ reduction was characterized by NH_3-TPD and the results are depicted in Fig. 9. Two desorption peaks can be observed on the profile of pure zeolite HZSM-5, and the peak located in the range of 120–275 °C (denoted as α peak) can be attributed to the weak acidic sites, while the peak located within the range of 275–500 °C (denoted as β peak), belongs to strong acid site (Mao et al., 2005, 2010). For the Cu-ZnO-ZrO_2/HZSM-5 catalysts, α peak and β peak shift respectively to a lower temperature and a higher temperature and the areas of both α peak and β peak become smaller. This result indicates that, compared with pure zeolite HZSM-5, the strength of the weak acid sites reduces while that of strong acid sites enhances, and the concentrations of both weak and strong acid sites decrease on the surface of the bifunctional catalysts. This can be due to the modification by oxalic acid during the preparation of bifunctional catalysts (Zhang et al., 2014b). In addition, for all the CZZH catalysts, the position and intensity of β peak are nearly the same, but those of α peak have a distinct difference. With the increase of calcination temperature, the temperature of α peak shifts to lower temperatures and its area becomes smaller, suggesting that both the strength and amount of the weak acid sites decrease.

Combining the results of NH_3-TPD characterization and catalytic testing, the similar methanol selectivity over the different bifunctional catalysts indicates that the acidity of each catalyst is enough to convert the formed methanol to DME. This result suggests that under the present reaction conditions the overall reaction over the bifunctional catalysts is determined by the methanol synthesis step rather than the DME formation itself (Mao et al., 2010).

3.5. *CO_2-TPD*

Fig. 10 shows the CO_2 desorption profiles obtained from the in situ reduced Cu-ZnO-ZrO_2/HZSM-5. Two CO_2 desorption peaks at low temperature (peak α) and high temperature (peak β) can be observed for all the samples, corresponding to CO_2 desorbed from a weak basic site and a strong basic site, respectively (Guo et al., 2010; Li et al., 2015; Xiao et al., 2015). The temperature of β peak maximum (370 °C) for different

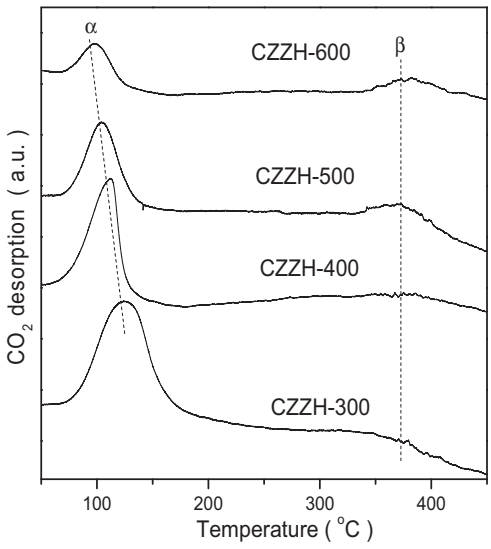

Fig. 10 – CO_2-TPD profiles of the pre-reduced CuO-ZnO-ZrO_2/HZSM-5 bifunctional catalysts.

Table 4 – Results of CO_2-TPD over the pre-reduced Cu-ZnO-ZrO_2/HZSM-5 bifunctional catalysts.

Catalyst	T_α (°C)	A_α (a.u.)
CZZH-300	126	124
CZZH-400	112	74
CZZH-500	102	53
CZZH-600	97	24

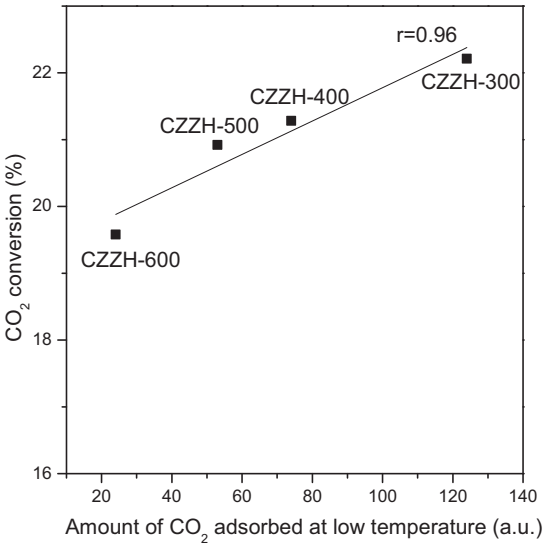

Fig. 11 – The relationship between CO_2 conversion and the amount of adsorbed CO_2 at low temperature.

catalysts has no noticeable change, indicating that the calcination temperature for catalyst preparation has inconspicuous effect on the strength of the strong basic site. The quantitative data of α peak over different catalysts are listed in Table 4. As seen, with the increase of calcination temperature, the peak position shifts from 126 to 97 °C and the amount of desorbed CO_2 decreases significantly from 124 to 24 (a.u.). This result indicates that both the strength and amount of weak basic sites of the Cu-ZnO-ZrO_2/HZSM-5 catalysts reduces with the increase in calcination temperature. Considering the reaction temperature used in the present work (250 °C), the CO_2 desorbed from low temperature (peak α) seems to be rather related with the active site for the methanol synthesis reaction than that from high temperature (peak β) because the temperature of peak β significantly exceeds 250 °C (Xiao et al., 2015). That means that the CO_2 adsorbed on strong sites is rather difficult to desorb under reaction conditions and might not take part in the reaction (Xiao et al., 2015; Wang and Zeng, 2005).

In this work, the relationship between the amount of CO_2 desorbed from low temperature and the conversion of CO_2 is illustrated in Fig. 11. It can be seen that the conversion of CO_2 increases almost linearly with the increment of the amount of CO_2 desorbed. Thus, the decreased CO_2 conversion over the bifunctional catalysts with the increase in calcination temperature is due to the decrease in amount of CO_2 desorbed from low temperature (Xiao et al., 2015).

3.6. *Comparison with other preparation methods*

Under the same reaction conditions, the DME yields over the CZZ(O) + HZ and CZZ(A) + HZ catalysts with the same composition but prepared by mechanical mixing method are 10.3% and 10.8%, respectively. This result indicates that the most efficient CZZH-300 catalyst prepared by the present one-step solid-state reaction method exhibits a remarkably higher catalytic performance (ca. 50% increment in DME yield) for direct DME synthesis from CO_2 hydrogenation than the ones prepared by the most widely used mechanical mixing method. On the other hand, similar catalysts were also studied in the literature. For example, a CuO-ZnO-ZrO_2/HZSM-5 catalyst with a mass ratio of 9:1 prepared by the one-step gel-oxalate precipitation-deposition method exhibited a DME yield of 8.6% at 240 °C, 3 MPa, $H_2/CO_2 = 3$, and GHSV = 2500 L kg_{cat}^{-1} h^{-1} (Frusteri et al., 2015b). In another paper (Zhang et al., 2014b) about a CuO-ZnO-ZrO_2/HZSM-5 catalyst with a mass ratio of 2:1 prepared by the same method as above, DME yield was increased to 15.9% at 270 °C, 3 MPa, $H_2/CO_2 = 3$, and GHSV = 4200 h^{-1}. Compared to these results, our catalyst seems to be promising, even if it needs to be further optimized. Moreover, the present solid-state reaction route is a simple, fast, environmentally friendly and energy-efficient method.

4. Conclusions

CuO-ZnO-ZrO_2/HZSM-5 bifunctional catalysts were synthesized via a route of solid-state reaction between hydrated metal salts and oxalic acid, which was found to be a simple, rapid and solvent-free method for the preparation of highly efficient bifunctional catalysts. The CuO-ZnO-ZrO_2 has an intimate contact with HZSM-5, so methanol can be dehydrated to form DME quickly after formation. The physicochemical properties and catalytic activity of the bifunctional catalysts are strongly influenced by the calcination temperature. With the increase of calcination temperature, the conversion of CO_2, selectivity and yield of DME all decrease due to the reduction of metallic copper surface area, adsorption capacity of CO_2, specific surface area, and reducibility of CuO.

Acknowledgments

The authors thank Shanghai Municipal Education Commission (13YZ117) and Science and Technology Commission of Shanghai Municipality (13ZR1441200) for financial supports.

References

Allahyari, S., Haghighi, M., Ebadi, A., Saeedi, H.Q., 2014. J. Power Sources 272, 929–939.
Arakawa, H., Dubois, J.-L., Sayama, K., 1992. Energy Convers. Manage. 33, 521–528.
Arena, F., Spadaro, L., Di Blasi, O., Bonura, G., Frusteri, F., 2004. Stud. Surf. Sci. Catal. 147, 385–390.
Bonura, G., Cordaro, M., Spadaro, L., Cannilla, C., Arena, F., Frusteri, F., 2013. Appl. Catal. B: Environ. 140–141, 16–24.
Bonura, G., Cordaro, M., Cannilla, C., Mezzapica, A., Spadaro, L., Arena, F., Frusteri, F., 2014. Catal. Today 228, 51–57.
Centi, G., Quadrelli, E.A., Perathoner, S., 2013. Energy Environ. Sci. 6, 1711–1731.
Frusteri, F., Cordaro, M., Cannilla, C., Bonura, G., 2015a. Appl. Catal. B: Environ. 162, 57–65.
Frusteri, F., Bonura, G., Cannilla, C., Drago Ferrante, G., Aloise, A., Catizzone, E., Migliori, M., Giordano, G., 2015b. Appl. Catal. B: Environ. 176–177, 522–531.
Fu, G.Y., Mao, D.S., Sun, S.S., Yu, J., Yang, Z.Q., 2015. J. Ind. Eng. Chem. 31, 283–290.
Ge, Q., Huang, Y., Qiu, F., Zhang, C., 1999. J. Nat. Gas Chem. 8, 280–285.
Guo, X.M., Mao, D.S., Lu, G.Z., Wang, S., Wu, G.S., 2009. Catal. Commun. 12, 1095–1098.

Guo, X.M., Mao, D.S., Lu, G.Z., Wang, S., Wu, G.S., 2010. J. Catal. 271, 178–185.
Jun, K., Shen, W., Rao, K., Lee, K., 1998. Appl. Catal. A: Gen. 174, 231–238.
Kondratenko, E.V., Mul, G., Baltrusaitis, J., Larrazábal, G.O., Pérez-Ramírez, J., 2013. Energy Environ. Sci. 6, 3112–3135.
Lee, K.H., Lee, J.S., 1995. Korean J. Chem. Eng. 12, 460–465.
Li, C., Yuan, X., Fujimoto, K., 2014. Appl. Catal. A: Gen. 469, 306–311.
Li, L., Mao, D.S., Yu, J., Guo, X.M., 2015. J. Power Sources 279, 394–404.
Liu, R.W., Qin, Z.Z., Ji, H.B., Su, T.M., 2013. Ind. Eng. Chem. Res. 52, 16648–16655.
Liu, R., Tian, H.F., Yang, A.M., Zha, F., Ding, J., Chang, Y., 2015. Appl. Surf. Sci. 345, 1–9.
Mao, D.S., Yang, W.M., Xia, J.C., Zhang, B., Song, Q.Y., Chen, Q.L., 2005. J. Catal. 230, 140–149.
Mao, D.S., Xia, J.C., Zhang, B., Lu, G.Z., 2010. Energy Convers. Manage. 51, 1134–1139.
Melián-Cabrera, I., López Granados, M., Fierro, J.L.G., 2002. J. Catal. 210, 273–284.
Najafabadi, A.T., 2013. Int. J. Energy Res. 37, 485–499.
Olah, G.A., 2013. Angew. Chem. Int. Ed. 52, 104–107.
Park, E., Nam, S.S., Choi, M.J., Lee, K.W., 1995. Energy Convers. Manage. 36, 573–576.
Pontzen, F., Liebner, W., Gronemann, V., Rothaemel, M., Ahlers, B., 2011. Catal. Today 171, 242–250.
Ribeiro, N.F.P., Souza, M., Schmal, M., 2008. J. Power Sources 179, 329–334.
Semelsberger, T.A., Borup, R.L., Greene, H.L., 2006. J. Power Sources 156, 497–511.
Shi, L., Shen, W., Yang, G., Fan, X., Jin, Y., Zeng, C., Matsuda, K., Tsubaki, N., 2013. J. Catal. 302, 83–90.
Słoczyński, J., Grabowski, R., Kozłowska, A., Olszewski, P., Stoch, J., Skrzypek, J., Lachowska, M., 2004. Appl. Catal. A: Gen. 278, 11–23.
Tao, J.L., Jun, K.W., Lee, K.W., 2001. Appl. Organometal. Chem. 15, 105–108.
Wang, J.Y., Zeng, C.Y., 2005. J. Nat. Gas Chem. 14, 156–162.
Wang, L.C., Liu, Y.M., Chen, M., Cao, Y., He, H.Y., Wu, G.S., Dai, W.L., Fan, K.N., 2007. J. Catal. 246, 193–204.
Wang, S., Mao, D.S., Guo, X.M., Lu, G.Z., 2009. Catal. Commun. 10, 1367–1370.
Wang, W., Wang, S., Ma, X., Gong, J., 2011. Chem. Soc. Rev. 40, 3703–3727.
Witoon, T., Permsirivanich, T., Kanjanasoontorn, N., Akkaraphataworn, C., Seubsai, A., Faungnawakij, K., Warakulwit, C., Chareonpanich, M., Limtrakul, J., 2015. Catal. Sci. Technol. 5, 2347–2357.
Xiao, J., Mao, D.S., Guo, X.M., Yu, J., 2015. Appl. Surf. Sci. 338, 146–153.
Ye, X., Jia, D., Yu, J., Xin, X., Xue, Z., 1999. Adv. Mater. 11, 941–942.
Zha, F., Ding, J., Chang, Y., Ding, J.F., Wang, J.Y., Ma, J., 2012. Ind. Eng. Chem. Res. 51, 345–352.
Zha, F., Tian, H., Yan, J., Chang, Y., 2013. Appl. Surf. Sci. 285, 945–951.
Zhang, M., Liu, Z., Lin, G., Zhang, H., 2013. Appl. Catal. A: Gen. 451, 28–35.
Zhang, Y.J., Li, D.B., Zhang, S.J., Wang, K.J., Wu, J., 2014a. RSC Adv. 4, 16391–16396.
Zhang, Y.J., Li, D.B., Zhang, Y., Cao, Y., Zhang, S.J., Wang, K.J., Ding, F., Wu, J., 2014b. Catal. Commun. 55, 49–52.